Defect-Tolerant Aligned Dipoles within Two-Dimensional Plastic Lattices

John C. Thomas,[†,‡] Jeffrey J. Schwartz,[‡,§] J. Nathan Hohman,[†,‡] Shelley A. Claridge,[†,‡,⊥] Harsharn S. Auluck,[†,‡] Andrew C. Serino,[‡,∥] Alexander M. Spokoyny,[†,¶] Giang Tran,[‡,#] Kevin F. Kelly,[‡,▽] Chad A. Mirkin,[*,¶] Jerome Gilles,[*,‡,#,○] Stanley J. Osher,[*,‡,#] and Paul S. Weiss[*,†,‡,∥]

[†]Department of Chemistry and Biochemistry, University of California, Los Angeles, Los Angeles, California 90095, United States, [‡]California NanoSystems Institute, University of California, Los Angeles, Los Angeles, California 90095, United States, [§]Department of Physics and Astronomy, University of California, Los Angeles, Los Angeles, California 90095, United States, [⊥]Department of Chemistry and Weldon School of Biomedical Engineering, Purdue University, West Lafayette, Indiana 47904, United States, [∥]Department of Materials Science and Engineering, University of California, Los Angeles, Los Angeles, California 90095, United States, [¶]Department of Chemistry and the International Institute for Nanotechnology, Northwestern University, Evanston, Illinois 60208, United States, [#]Department of Mathematics, University of California, Los Angeles, Los Angeles, California 90095, United States, [▽]Department of Electrical and Computer Engineering, Rice University, Houston, Texas 77005, United States, and [○]Department of Mathematics and Statistics, San Diego State University, San Diego, California 92182, United States

ABSTRACT Carboranethiol molecules self-assemble into upright molecular monolayers on Au{111} with aligned dipoles in two dimensions. The positions and offsets of each molecule's geometric apex and local dipole moment are measured and correlated with sub-Ångström precision. Juxtaposing simultaneously acquired images, we observe monodirectional offsets between the molecular apexes and dipole extrema. We determine dipole orientations using efficient new image analysis techniques and find aligned dipoles to be highly defect tolerant, crossing molecular domain boundaries and substrate step edges. The alignment observed, consistent with Monte Carlo simulations, forms through favorable intermolecular dipole—dipole interactions.

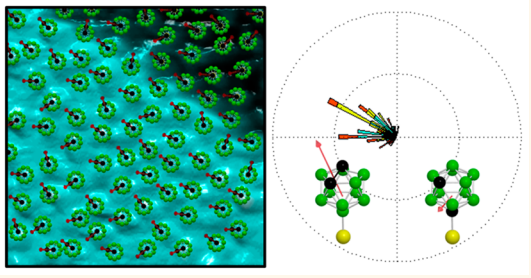

KEYWORDS: nanoscience · self-assembly · carborane · self-assembled monolayer · dipole alignment · scanning tunneling microscopy · two-dimensional · ferroelectric · defect tolerant

Engineering molecular systems with precisely determined positions, orientations, and interactions enables control over chemical reactions[1] with implications for catalysis, nanomaterials engineering, and bioassembly.[2−7] Molecular dipole alignment has been demonstrated using strong electrostatic fields, collisional forces, and intense laser fields.[8−11] Most alignment characterization methods are ensemble measurements, where local information is lost through averaging.[12−14] The promise of using scanning tunneling microscopy (STM) to resolve chemical state information, at the single-molecule scale, beyond structure, has spurred the development of a plethora of technique extensions, including photon-coupled, alternating current, and microwave-coupled STM.[1,15−22] We employ multimodal STM to visualize molecular alignment of dipole-containing carboranethiolate within self-assembled monolayers (SAMs) at 4 K. We measure local barrier height (LBH) as a function of position across the surface by modulating the tip—surface separation distance (z) around its constant-current (I) topographic imaging value, which is a convolution of both topographic and electronic information. The first harmonic (dI/dz) of the modulated current is mapped as the LBH of the sample, which is related to the local work function.[23−26] This enables simultaneous measurements of the local dipoles and the exposed interface to visualize molecular orientations within simple two-dimensional systems. Here, we observe molecular alignment spanning areas of $\sim 10^3$ Å^2, driven by dipole—dipole interactions within SAMs. These long-range interactions, proportional to the inverse cube of the dipole separation ($\propto r^{-3}$) and therefore outside the purview of the Mermin-Wagner theorem,[27,28] support azimuthal molecular ordering. Measurements are recorded using a custom-built, ultrastable microscope.[29] We use STM to determine the

* Address correspondence to psw@cnsi.ucla.edu, chadnano@northwestern.edu, jegilles@mail.sdsu.edu, sjo@math.ucla.edu.

Received for review November 21, 2014 and accepted April 13, 2015.

Published online April 13, 2015
10.1021/acsnano.5b01329

interplay between molecular geometry and intermolecular interactions.

Self-assembly provides a convenient platform for the construction of well-defined monomolecular films, with applications ranging from nanotechnology to the life sciences.[30−35] While the more commonly used *n*-alkanethiols in monolayers tilt and have many conformational degrees of freedom that lead to defects, carboranethiols are rigid, three-dimensional carbon−boron-hydrogen cage compounds that adsorb upright and readily form ordered monolayers on gold.[36,37] Since carboranethiols on Au{111} form identical monolayer lattices independent of isomer, they provide simple systems with which to test the effects of intermolecular interactions without varying monolayer structure.[38,39] Motivated by the observation that, at room temperature, carboranethiols with dipole components parallel to the surface outcompete those with dipoles normal to the surface, we sought to observe directly the intermolecular dipole interactions most likely to be responsible for this effect. Conventional STM enables the determination of the positions of individual molecules, but not the orientation nor rotation in azimuthally symmetric systems. Here, carboranethiol isomers contain symmetric backbones and many have significant dipoles, but appear topographically symmetric in STM measurements. As noted above, we inferred that the results of the competitive binding of carboranethiol isomers were due to dipolar interactions, but it was not possible to resolve the orientations of individual symmetric molecules such as carboranethiols until now. We use STM topographic and spectroscopic imaging to measure topography and the spatial dipole orientation, simultaneously, with submolecular resolution. We compare and contrast monolayers of *o*-9-carboranethiolate (**O9**) and *m*-1-carboranethiolate (**M1**); the largest local contribution to charge separation is from the electron-deficient carbon atoms in the *ortho* and *meta* positions, respectively. We then correlate topographic maxima with the tunneling barrier-height extrema to measure the dipole offset within different regions, molecular domains, substrate terraces, and molecules within the SAMs.

Monolayers of carboranethiols and other upright symmetric cage molecules have lattices determined by the projections of the cages on the substrate surface.[37,39−41] Thus, the **O9** and **M1** carboranethiol SAMs have identical lattices. The most common defects in these monolayers are substrate step edges and molecular domain boundaries in which there is a translational (phase) and/or rotational offset of the registry of the lattice of attachment to the substrate.[37,39,40,42,43]

RESULTS AND DISCUSSION

Topographic and LBH modalities are measured simultaneously. We image domains in **O9** monolayers (Figure 1A−C) and compare local molecular dipole orientations across monatomic substrate steps (Figure 1E,F). Local extrema in both modalities are computed within a square pixel window having a width of the approximate nearest neighbor spacing (∼7.2 Å). Variations in the tunneling LBH, $\varphi = 0.95(\mathrm{d}\ \ln(I)/\mathrm{d}z)^2$, are related to variations in the local molecular dipole,[44−46] enabling the association of LBH extrema to the substrate dipole signal maxima or minima, while topographic maxima correspond to molecular apexes. The **O9** molecule was designed to contain a large dipole (5.72 D) that is tilted off normal with respect to the underlying substrate surface (see Supporting Information for synthesis and molecular dipole computation) and we assign LBH minima as the local work function signal minima due to *o*-carbon atoms. Topographic and LBH extrema are overlaid, and the offsets between them are evaluated *via* block-matching[47,48] to compute correlations between sliding image patches in both bounded modalities within a molecular-sized search window (Figure 2). Rose plots are circular histograms that we use here to depict the dipole offsets from topographic maxima, binned by orientation and magnitude. We include multiple domains using image thresholding and masking techniques to test the extent to which dipole orientation depends on the structural features of the molecular lattices (Figure 3). The analysis of dipole direction across a Au{111} step edge reveals aligned molecular orientations of 154 ± 28° on the upper terrace and 160 ± 22° on the lower terrace, where angles are always reported with respect to the (horizontal, fast-scan direction) image axis of both topography and LBH. Supporting Information Figure S1 highlights two groupings of molecules within the same area examined in Figure 1, where the local dipole orientations are measured to be 49 ± 5° and 156 ± 28°. Different dipole orientations have been observed in the same multimodal image pairs, but are uncommon. This defect tolerance of dipole alignment with regard to structural domain boundaries and substrate step edges is discussed further below.

We contrast molecular **O9** orientation measurements with those made on SAMs of **M1**, which possess the same lattice structure.[39] Molecular dipoles of **M1** (1.06 D) are smaller in magnitude, with the largest component oriented in the plane of the substrate. The LBH minima measured correspond to the electron-deficient carbon atoms at both the 1- and 2-positions within **O9** monolayers and the 1- and 7-carbon atoms within **M1** monolayers. The same analyses, in which topographic maxima and LBH minima are overlaid and correlations are computed, are performed for regions of **M1** SAMs, and orientations are mapped within single atomically flat terraces of gold (Figure 4). In Figure 4, three regions are highlighted by inspection, where two are lattice matched with different orientations and the third is a region of local disorder, as confirmed by Fourier analysis of the segmented domains

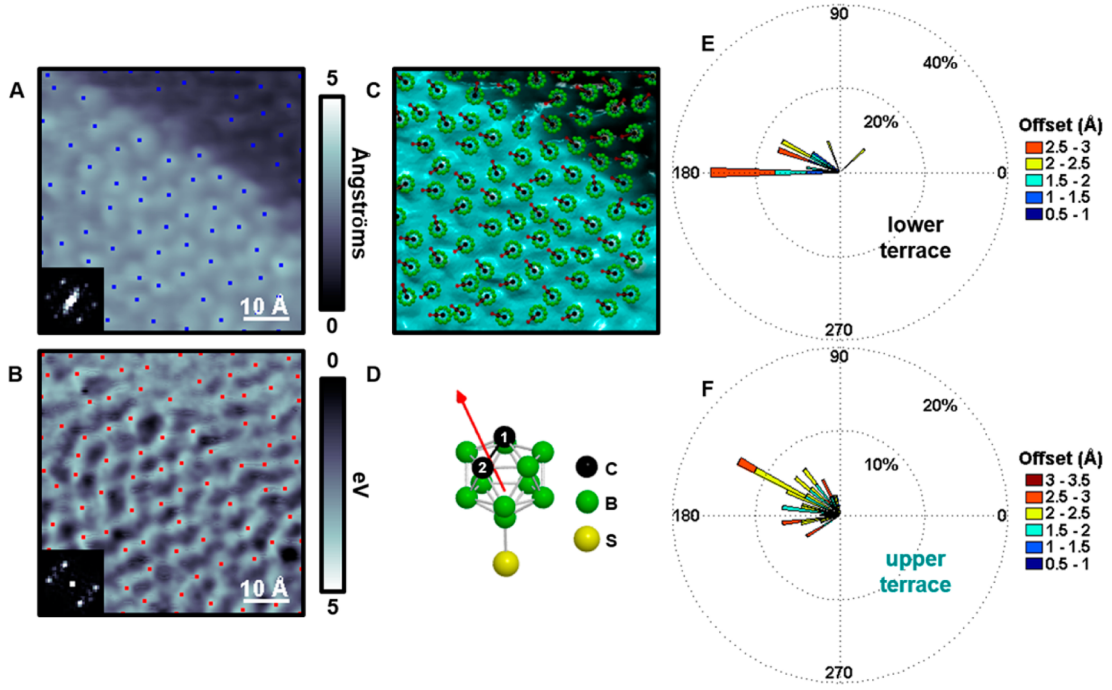

Figure 1. (A) Scanning tunneling topograph ($I_{tunneling}$ = 15 pA, V_{sample} = −0.5 V) of *o*-9-carboranethiol (O9) on Au{111} along a monatomic substrate step edge with local maxima (blue) depicted. Inset depicts a fast Fourier transform (FFT), corroborating a hexagonally close-packed arrangement with a nearest-neighbor spacing of 7.2 ± 0.4 Å. (B) Simultaneously acquired local barrier height (LBH) image, which is inverted to highlight dipole orientations, with computed local maxima (red). Inset depicts a FFT revealing the order seen topographically. (C) Schematic displaying topography and computed molecular orientations. (D) A ball-and-stick model of O9 that contains a calculated dipole magnitude of 5.72 D, where hydrogen atoms are omitted for clarity. Rose plots (depicting dipole offsets) of the lower terrace (E) and upper terrace (F) that are binned by both magnitude (0.5 Å bins) and orientation (4° bins). Angles reported are given with respect to the fast-scan direction, shown as horizontal, in the STM images.

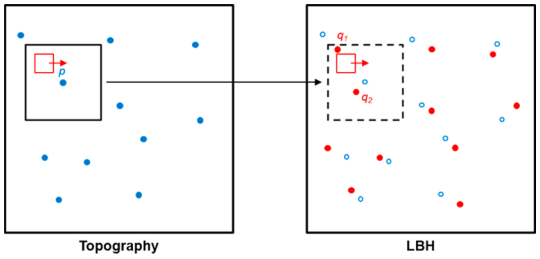

Figure 2. With two corresponding sets of local maxima per data set (the blue dots in the topography image and the red dots in the local barrier height, LBH, image), a maximum *p* from the topography image is selected and we search for its corresponding LBH maximum using a block-matching approach. Since both scanning tunneling microscopy modalities are acquired simultaneously, the two images are bounded, and we can define a search window (the black square in the topography image and dotted black square in the LBH image) centered at *p* of a given dimension (size of one molecule). Next, we compute the correlation between sliding patches taken at the same position in each image within the search window. Among the LBH maxima candidates (*i.e.*, q_1 and q_2) that correspond to *p*, we choose the one with highest correlation. We perform this procedure for each maximum *p* in the topographic image and finally compute a set of vectors (dipole positions with respect to molecular maxima) associated with each molecule.

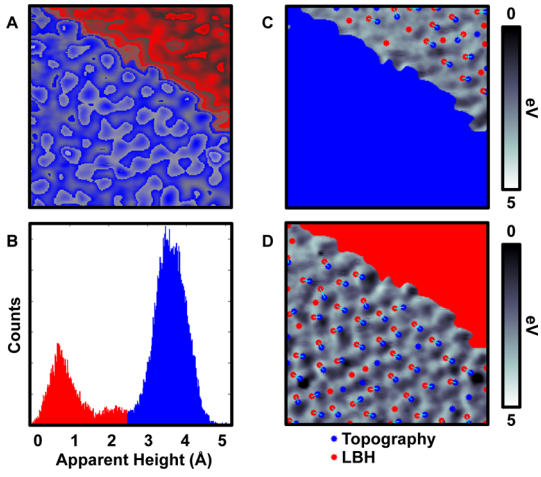

Figure 3. We bifurcate the topographic image along a monatomic Au{111} step edge (A) and show the image histogram in B. Here, we separate the upper (blue) and lower (red) terrace in topography based on thresholding and create a mask that is used to segment LBH images. Topographic and LBH extrema are overlaid for both the lower terrace (C) and upper terrace (D), and correlations are computed. Both (C) and (D) show dipole offsets used for the Rose plots in Figure 1.

(Supporting Information Figure S2). As noted previously, the domain boundaries in complete monolayers of upright symmetric cage molecules are simpler and more difficult to identify than those of the more common alkanethiols and other linear, tilted molecules with conformational degrees of freedom.[39,40] This simplicity is the result of having only rotational and translational lattice offsets between neighboring domains.

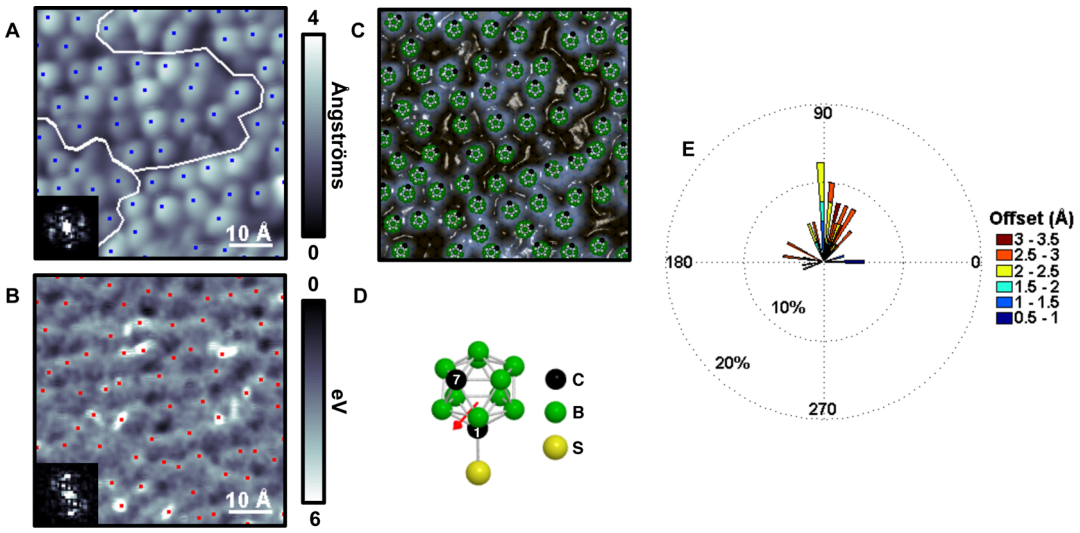

Figure 4. (A) Scanning tunneling topograph ($I_{tunneling}$ = 15 pA, V_{sample} = −0.5 V) of *m*-1-carboranethiol (M1) on Au{111} on a single Au terrace with lines separating three different regions (see Supporting Information Figure S2 for further explanation). Inset depicts the fast Fourier transform, revealing a hexagonally close-packed arrangement with a 7.2 Å nearest-neighbor spacing. Local maxima of both topographic (A) and inverted local barrier height (B) are computed. (C) A schematic displaying molecular position overlaid with topography. (D) A ball-and-stick model of M1 that contains a dipole (1.06 D) oriented mainly in the plane of the gold substrate, where hydrogen atoms are omitted for clarity. (E) Rose plot of measured dipole vector orientations binned by both magnitude (0.5 Å bins) and orientation (4° bins). (See Supporting Information Figure S7 for correlation results used in panel E.) Angles reported are given with respect to the fast-scan direction, shown as horizontal, in the STM images.

In the analyzed regions shown, dipoles are oriented 88 ± 47° with respect to the (horizontal, fast-scan direction) image axis. For both carboranethiol monolayers, defect-tolerant alignment is observed across both substrate step edges and molecular domain boundaries. This is further demonstrated over 44 h of imaging, where aligned orientations (63 ± 45°) are measured although separated by a monatomic Au{111} substrate step (see Supporting Information, video). We observe that, like the molecular structural domain boundaries, the relatively small spatial offset of the substrate step is transited by dipole−dipole interactions, leading to dipole alignment that cross these interfaces.

Correlations are computed using sliding patches taken at the same positions in each image window for each maximum *p* in the topographic images and each maximum *q* in the LBH images. We obtain a set of vectors, *pq*, associated with each dipole. Our analysis shows that the lateral offset measured within **O9** monolayers is 2.0 ± 0.4 Å, as depicted in Figure 1. Correlated local topographic maxima and LBH minima of **M1** SAMs reveal a local offset of 2.3 ± 0.7 Å in Figure 4. Across many samples and images ($n_{molecules}$ > 1000), **O9** displays an average offset of 1.9 ± 0.5 Å and **M1** shows an average offset of 1.9 ± 0.6 Å. Recently, long-range dipolar interactions of carboranethiol isomers across aqueous media were observed, where molecular dipoles oriented parallel to the surface experience stronger intermolecular interactions that those oriented normal to the surface, likely due to the correlation of lateral surface dipoles.[49] Density functional theory is employed to extrapolate a point dipole that is used to predict alignment (see Supporting Information).

We apply a simple model to determine the dipole−dipole interaction energies within a SAM and use it to understand the observed data (Figure 5). In brief, we define each molecule's dipole interaction energy as the potential energy of its calculated dipole moment in the local electric field it experiences. The in-plane component of the electric field from the tip is insignificant in the tunneling junction; thus, we do not include tip-induced electric field effects in our calculations. This assumption is tested experimentally and confirmed, where molecular orientations remain fixed in space, independent of scan direction, for over 44 h of imaging at low temperature (see Figure S3 and Supporting Information). In our model, the surrounding molecules, assumed to be ideal electric dipoles arranged in a hexagonal lattice, determine the field's strength and direction. Alignment with (against) the field acts to stabilize (change) the dipole orientations. Using this model, we estimate the molecules' interaction energies, and changes in those energies, resulting from dipole reorientations with respect to the surrounding SAM lattice. To determine possible stable orientations of molecular dipoles in a SAM, we employ a Monte Carlo method using the Metropolis algorithm[50] and the interaction energies described above. When the temperature is sufficiently low, we find that the system spontaneously evolves toward a state in which the dipoles align along a common direction, as illustrated in Figure 6. The favorable dipole alignment energy

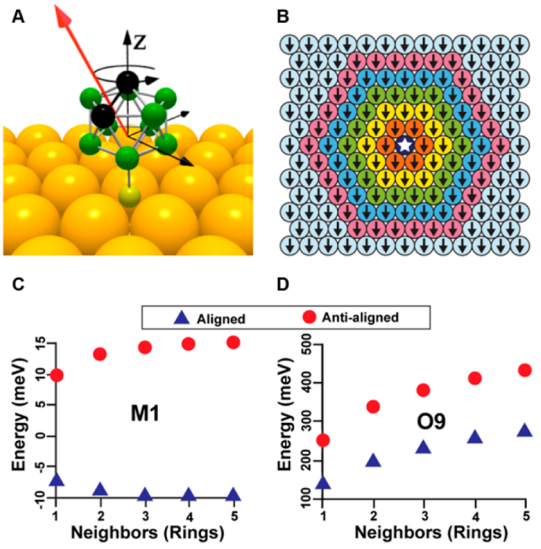

Figure 5. Dipole interaction energy. To estimate the dipole interaction energy, we consider carboranethiol molecules standing normal to a gold surface, along the *z*-axis, as shown in the perspective model (A) of an *o*-9-carboranethiol (O9) molecule. Iterations of the Metropolis algorithm affect random rotations about the *z*-axis, changing the dipole (red arrow) orientation and interaction energy. (B) Representation of a carboranethiol self-assembled monolayer in which each inscribed arrow indicates the in-plane orientation of a molecular dipole. Here, every dipole in the molecular lattice, except that of the central molecule, aligns along the same direction, toward the bottom of the figure. Plots (C) and (D) show the interaction energies of a dipole aligned in the same ("aligned", blue triangles) and opposite ("anti-aligned", red circles) direction as that of its neighbors, in the cases of *m*-1-carboranethiol (M1) and O9 monolayers, respectively. The interaction energy depends on the number of concentric, hexagonal rings of neighboring molecules. In (B), we highlight the first five rings around a central molecule (indicated by an inscribed star) with the colors orange, yellow, green, blue, and pink. Molecules outside the considered rings do not contribute to the interaction energy.

stabilizes their orientations and promotes the formation and growth of locally ordered regions of molecular dipoles. These results are consistent with the STM topographic and LBH data discussed above and explain the mechanism driving dipole ordering. We expect the transition temperature for the observed molecular alignment occurs between 4 and 293 K, as suggested by our model, but we have neither determined this transition temperature experimentally nor performed temperature-dependent simulations.

Scanning tunneling microscopy can image both molecular overlayers and substrate atoms to make absolute tilt assignments in the case where the molecule−substrate bonds determine the largest dipoles.[26,51] Our measurements, instead, use LBH imaging with molecules possessing a permanent dipole to resolve local orientation within the SAM's chemical environment for the first time. Both topographic and LBH images, 256 × 256 pixels, are initially corrected for image aberrations, caused by residual drift and non-orthogonalities of the scanner tube during the time allotted for high-resolution data acquisition (~2 h), on a line-by-line basis using a matrix transformation approach (Supporting Information Figures S4 and S5). Shear distortions are accounted for in Fourier space, and the corrected images are used in further analyses. Local barrier height images are inverted for clarity and local extrema are overlaid (Supporting Information Figures S6 and S7); we then connect each topographic maximum to all LBH maxima within a square pixel window as a function size and compare these results to the computed correlations, described above, for both molecular monolayers. In both **O9** and **M1** images shown, the block-matching approach yields the maximum computed correlation, while connecting all extrema in a square pixel window, as a function of size, exhibits increased artifacts. We also compare entropy metrics, quantified in MATLAB (Supporting Information Figures S8 and S9), within local regions in **O9** monolayers and in **M1** monolayers. When entropy grayscale values are measured in each 9 × 9 pixel neighborhood, centered at each pixel, mean entropy values in both topographic and LBH image masks contain a large number (256) of accessible values and therefore demonstrate higher image textural contrast in comparison to binary images (with only two possible values) with mean entropy grayscale values near zero.[52] In previous work, near continuous modulation of the metal work function of ~1 eV was attained with controlled mixtures of carboranethiol isomers and these monolayers were shown to be robust with respect to coverage with active organic layers in fabricated devices.[53] Local barrier heights in the figures above show similar modulation of the work function with respect to Au{111}. The analysis and segmentation techniques described here are used to identify the (lattice registry) domains of the carboranethiolates in addition to the dipole orientations within and between domains.[54−56] Data acquisition coupled with new image analysis techniques enable understanding of local snapshots between bounded topographically exposed and dipole interfacial modalities.

CONCLUSIONS AND PROSPECTS

This multimodal imaging procedure permits the measurement of molecular orientations by correlating topographic and LBH images. Carboranethiols are a fruitful system for study, in that both pure **M1** and **O9** form monolayers containing fewer types and number of defects compared to assemblies of linear and/or tilted molecules with conformational and orientational degrees of freedom,[37,39,57−60] and contain a large molecular dipole originating from their rigid cage. Isomeric carborane systems may find applications in the fields of molecular machines, dipolar rotors, and functionalized coatings for device

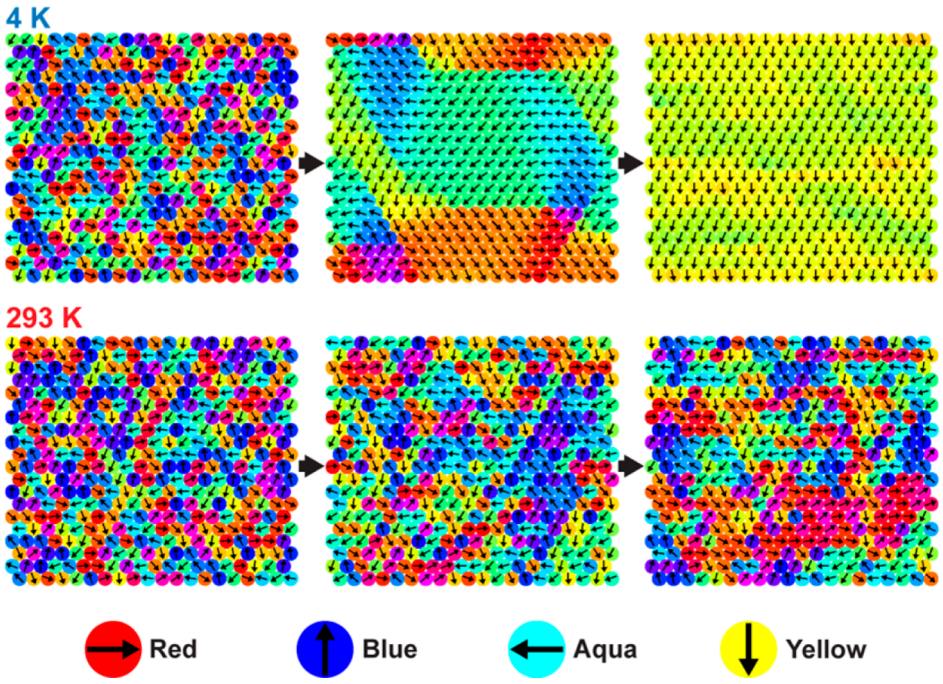

Figure 6. Simulated monolayers evolving under the influence of internal dipole fields. We track the orientation of molecular dipoles in a 20 × 20 molecule region of a self-assembled *o*-9-carboranethiol (O9) monolayer. At 4 K (top), the molecular dipoles evolve toward a state in which they align along a common direction. However, we do not observe this trend in simulations at 293 K (bottom); the dipoles remain randomly oriented and no permanent polarization develops. The sequences depict initial (left), intermediate (middle), and final (right) states of the monolayer over the course of 500 000 iterations of a Monte Carlo algorithm. Here, we represent individual O9 molecules as circles inscribed with an arrow indicating the orientation of the molecule's in-plane dipole moment. The dipole orientation also determines the depicted color of each molecule. Molecules with dipoles oriented toward the top (bottom) of the figure appear blue (yellow), whereas molecules with dipoles oriented left (right) appear aqua (red); intermediate orientations result in combinations of these colors. Monolayers composed of *m*-1-carboranethiol molecules evolve in a similar way to those of O9. (See Supporting Information, video.)

frameworks.[49,52,61,62] Scanning tunneling microscopy is able to probe the exposed two-dimensional interfaces in topographic mode and the corresponding buried dipole interface in LBH mode, simultaneously. We have successfully determined molecular orientation within azimuthally symmetric carboranethiolate monolayers. We have found that dipole alignment crosses domain boundaries and substrate steps. These results are consistent with the preference for adsorption of carboranethiols with dipole components lateral to the surface over those with dipoles normal to the surface observed in competitive adsorption from mixed solutions.[39]

Creating monolayer systems with defect tolerance and precisely determined dipoles enables greater tunability of assemblies with enhanced control of stability through designed interactions. Other single-molecule measurement techniques are hindered by either extreme dilution or specificity, whereas STM can measure the local environment with submolecular resolution and use spectroscopic imaging for chemical identification.[17,61−67] We anticipate that determining and structuring chemical environments with cage-molecule assemblies will be important in creating atomically precise structures in two and three dimensions.

MATERIALS AND METHODS

Self-Assembled Monolayer Preparation. Benzene and **M1** were used as received (Sigma-Aldrich, St. Louis, MO). The chemical **O9** was synthesized and characterized in accordance with previously published methods.[43] The Au{111}/mica substrates (Agilent Technology, Tempe, AZ) were hydrogen-flame-annealed prior to SAM formation with 10 passes at a rate of 0.4 Hz. Both SAMs were prepared by immersion into 1 mM solutions in benzene, held at room temperature, for approximately 10 min. Short deposition times were employed to increase the occurrence of local defects and still obtain a well-ordered monolayer. After deposition, each sample was rinsed thoroughly with neat benzene, dried under a stream of ultrahigh purity argon, and then inserted into the ultrahigh vacuum chamber for analysis.

Nanoscale Imaging. All STM measurements were performed with a custom-built Besoke-style scanning tunneling microscope held at cryogenic (4 K) and extreme high vacuum ($<10^{-12}$ Torr) conditions.[68] Samples were held at a fixed bias ($V_{sample} = -0.5$ V) and both topographic and LBH modalities were measured in a constant current fashion ($I_t = 15$ pA). The tunneling-gap distance was modulated at a frequency above the microscope feedback loop bandwidth (~3 kHz) with a sinusoidal amplitude (dz ~0.1 Å) and dI/dz was measured with

a lock-in technique (Stanford Research Systems SR850 DSP, Sunnyvale, CA). The well-known lattice of atomic Au{111}, held at 4 K, was measured and used to calibrate all images. The measured LBH magnitude may vary in cases where the applied voltage does not exactly equal the voltage across the tunneling junction.[45,69] With this condition in mind, local barrier height micrographs were calibrated against Au step edge measurements to verify the procedure used (Supporting Information Figure S10).

Image Analyses. All STM images were processed and matrix-smoothed with automated routines developed in MATLAB (Mathworks, Natick, MA) to remove any high-frequency noise and intensity spikes that may otherwise impair reliable extrema selection.[26] Images were then skew-corrected and checked in Fourier space to remove any image aberrations due to drift and piezoelectric transducer nonlinearities. We denote points p and q as local maxima in topographic and inverted LBH images, respectively. A point p was considered a local maximum if its intensity was greater than that of all surrounding pixels within a molecular-sized neighborhood of radius ws; the same method was used to compute each point q in the LBH image. After the sets of points p and q were obtained, an image patch centered at each p, of the size $[2ps + 1] \times [2ps + 1]$, was correlated at each pixel against a larger LBH image patch, centered at q, of the size $[2qs + 1] \times [2qs + 1]$. Parameter qs is the size of the next-nearest neighbor spacing, and parameter ps is the size of one molecule. This technique is referred to as block-matching that has established use in the fields of image compression and object recognition.[47,48,70,71] The maximum correlation was chosen for each point p to q, which was then referenced and plotted.

Dipole−Dipole Interaction Energy. We modeled each carboranethiol molecule as an ideal electric dipole moment located at the center of its cage moiety in a hexagonally close-packed array. We estimated a molecule's dipole interaction energy to be the electric potential energy (U) of the molecule's dipole moment ($\vec{p}$) in the local electric field ($\vec{E}$),

$$U = -\vec{p} \cdot \vec{E}$$

The electric field is the vector sum of the fields produced by the surrounding dipoles

$$\vec{E} = \sum_i \frac{1}{4\pi\epsilon_0} \frac{3(\vec{p}_i \cdot \vec{r})\vec{r} - \vec{p}_i}{r^3}$$

where r represents the separation distance between the molecule under consideration and its ith neighboring dipole moment ($\vec{p}_i$). The gold substrate also influences the electric field due to the induced charge on the conductor, effectively producing an image dipole beneath the surface for each dipole in the SAM. The dipole interaction strength diminishes as r^{-3}, making more distant dipole moments less significant contributors to the calculated energy. Accordingly, the summation above includes only the neighboring molecular dipoles, and image dipoles, contained within the first four concentric, hexagonal rings surrounding the considered molecule. Finally, we assumed left−right and top-bottom periodicity in our modeled SAM, such that opposite edges of the rectangular molecular lattice coincided, and thus simulated an infinite monolayer.

Monte Carlo Simulations. We used the Metropolis algorithm to determine possible equilibrium orientations of molecular dipole moments within a SAM. Iteratively, the interaction energy of a randomly chosen molecule within a SAM was computed before and after a proposed reorientation. Each reorientation rotated the molecule by a random angle about an axis normal to the substrate, thereby only altering the lateral position and in-plane components of the dipole moment. Depending on the change in energy, the reorientation was either accepted and preserved in subsequent iterations, or discarded without changing the state of the system. The probability of preserving the change is

$$\text{Probability}(\%) = 100 \times \begin{cases} 1, \Delta E < 0 \\ e^{-\Delta E/k_B T}, \Delta E \geq 0 \end{cases}$$

where ΔE is the change in the dipole interaction energy due to the reorientation, T is the absolute temperature of the system, and k_B is the Boltzmann constant.

We initialized a model SAM to have no net in-plane polarization (randomized molecular azimuths) and allowed it to evolve through successive iterations. Our simulations predict that, at the low temperatures used experimentally (4 K), both **O9** and **M1** SAMs evolve toward states with regions of locally aligned in-plane molecular dipoles, as shown in the STM data. However, we did not observe spontaneous dipole ordering near room temperature (~293 K) and, furthermore, note the loss of order in a prealigned SAM due to random thermal reorientations.

Conflict of Interest: The authors declare no competing financial interest.

Supporting Information Available: Figures that depict local dipole offset along domains, sample directional dependence, aberration corrections, image correlation, pixel entropy, calibration used, script, dipole computation, and movies that show local barrier height as a function of time and Monte Carlo simulations. This material is available free of charge *via* the Internet at http://pubs.acs.org.

Acknowledgment. We thank the DoE DE-SC-0005025 for support of the instrumentation and methods developed and applied here and the W. M. Keck Foundation for support of the analysis methods developed and used. The synthetic aspects of this work were supported by AFOSR award FA9550-07-1-0534 and ARO award W911NF-06-1-0116 to CAM. AMS gratefully acknowledges the support of a Northwestern University 2011 Presidential Fellowship. We gratefully thank Adam Kurland, Patrick Han, David McMillan, and Greg Pawin for their support and guidance.

REFERENCES AND NOTES

1. Kim, M.; Hohman, J. N.; Cao, Y.; Houk, K. N.; Ma, H.; Jen, A. K.; Weiss, P. S. Creating Favorable Geometries for Directing Organic Photoreactions in Alkanethiolate Monolayers. *Science* **2011**, *331*, 1312–1315.
2. Jorgensen, W. L.; Swenson, C. J. Optimized Intermolecular Potential Functions for Amides and Peptides. Structure and Properties of Liquid Amides. *J. Am. Chem. Soc.* **1985**, *107*, 569–578.
3. Friedrich, B.; Herschbach, D. Alignment and Trapping of Molecules in Intense Laser Fields. *Phys. Rev. Lett.* **1995**, *74*, 4623–4626.
4. Zhang, Y.; Chang, A.; Cao, J.; Wang, Q.; Kim, W.; Li, Y.; Morris, N.; Yenilmez, E.; Kong, J.; Dai, H. Electric-Field-Directed Growth of Aligned Single-Walled Carbon Nanotubes. *Appl. Phys. Lett.* **2001**, *79*, 3155–3157.
5. Stapelfeldt, H. Colloquium: Aligning Molecules with Strong Laser Pulses. *Rev. Mod. Phys.* **2003**, *75*, 543–557.
6. Mandal, S. K.; Okawa, Y.; Hasegawa, T.; Aono, M. Rate-Determining Factors in the Chain Polymerization of Molecules Initiated by Local Single-Molecule Excitation. *ACS Nano* **2011**, *5*, 2779–2786.
7. Okawa, Y.; Aono, M. Materials Sciene: Nanoscale Control of Polymerization. *Nature* **2011**, *409*, 683–684.
8. Estler, R. C.; Zare, R. N. Laser-Induced Chemiluminescence: Variation of Reaction Rates with Reagent Approach Geometry. *J. Am. Chem. Soc.* **1978**, *100*, 1323–1324.
9. Loesch, H. J.; Remscheid, A. Brute Force in Molecular Reaction Dynamics: A Novel Technique for Measuring Steric Effects. *J. Chem. Phys.* **1990**, *93*, 4779–4790.
10. Baugh, D. A.; Young Kim, D.; Cho, V. A.; Pipes, L. C.; Petteway, J. C.; Fuglesang, C. D. Production of a Pure, Single Ro-Vibrational Quantum-State Molecular Beam. *Chem. Phys. Lett.* **1994**, *219*, 207–213.
11. Pirani, F.; Cappelletti, D.; Bartolomei, M.; Aquilanti, V.; Scotoni, M.; Vescovi, M.; Ascenzi, D.; Bassi, D. Orientation of Benzene in Supersonic Expansions, Probed by IR-Laser Absorption and by Molecular Beam Scattering. *Phys. Rev. Lett.* **2001**, *86*, 5035–5038.

12. Brooks, P. R.; McKillop, J. S.; Pippin, H. G. Molecular Beam Reaction of K Atoms with Sideways Oriented CF_3I. *Chem. Phys. Lett.* **1979**, *66*, 144–148.
13. Aquilanti, V.; Ascenzi, D.; Cappelletti, D.; Pirani, F. Velocity Dependence of Collisional Alignment of Oxygen Molecules in Gaseous Expansions. *Nature* **1994**, *371*, 399–402.
14. Weida, M. J.; Parmenter, C. S. Aligning Symmetric and Asymmetric Top Molecules *via* Single Photon Excitation. *J. Chem. Phys.* **1997**, *107*, 7138–7147.
15. Berndt, R.; Gaisch, R.; Gimzewski, J. K.; Reihl, B.; Schlittler, R. R.; Schneider, W. D.; Tschudy, M. Photon Emission at Molecular Resolution Induced by a Scanning Tunneling Microscope. *Science* **1993**, *262*, 1425–1427.
16. Stranick, S. J.; Weiss, P. S. Alternating Current Scanning Tunneling Microscopy and Nonlinear Spectroscopy. *J. Phys. Chem.* **1994**, *98*, 1762–1764.
17. McCarty, G. S.; Weiss, P. S. Scanning Probe Studies of Single-Nanostructures. *Chem. Rev.* **1999**, *99*, 1983–1990.
18. Donhauser, Z. J.; Mantooth, B. A.; Kelly, K. F.; Bumm, L. A.; Monnell, J. D.; Stapleton, J. J.; Price, D. W., Jr.; Allara, D. L.; Tour, J. M.; Weiss, P. S. Conductance Switching in Single Molecules through Conformational Changes. *Science* **2001**, *292*, 2303–2307.
19. Wu, S. W.; Ogawa, N.; Ho, W. Atomic-Scale Coupling of Photons to Single-Molecule Junctions. *Science* **2006**, *312*, 1362–1365.
20. Claridge, S. A.; Schwartz, J. J.; Weiss, P. S. Electrons, Photons, and Force: Quantitative Single-Molecule Measurements from Physics to Biology. *ACS Nano* **2011**, *5*, 693–729.
21. Giridharagopal, R.; Zhang, J.; Kelly, K. F. Antenna-Based Microwave Frequency Scanning Tunneling Microscope System. *Rev. Sci. Instrum.* **2011**, *82*, 053710.
22. Bonnell, D. A.; Basov, D. N.; Bode, M.; Diebold, U.; Kalinin, S. V.; Madhavan, V.; Novotny, L.; Salmeron, M.; Schwarz, U. D.; Weiss, P. S. Imaging Physical Phenomena with Local Probes: From Electrons to Photons. *Rev. Mod. Phys.* **2012**, *84*, 1343–1381.
23. Lang, N. D. Apparent Barrier Height in Scanning Tunneling Microscopy. *Phys. Rev. B* **1988**, *37*, 10395–10398.
24. Zheng, X.; Mulcahy, M. E.; Horinek, D.; Galeotti, F.; Magnera, T. F.; Michl, J. Dipolar and Nonpolar Altitudinal Molecular Rotors Mounted on an Au(111) Surface. *J. Am. Chem. Soc.* **2004**, *126*, 4540–4542.
25. Monnell, J. D.; Stapleton, J. J.; Dirk, S. M.; Reinerth, W. A.; Tour, J. M.; Allara, D. L.; Weiss, P. S. Relative Conductances of Alkaneselenolate and Alkanethiolate Monolayers on Au{111}. *J. Phys. Chem. B* **2005**, *109*, 20343–20349.
26. Han, P.; Kurland, A. R.; Giordano, A. N.; Nanayakkara, S. U.; Blake, M. M.; Pochas, C. M.; Weiss, P. S. Heads and Tails: Simultaneous Exposed and Buried Interface Imaging of Monolayers. *ACS Nano* **2009**, *3*, 3115–3121.
27. Mermin, N. D.; Wagner, H. Absence of Ferromagnetism or Antiferromagnetism in One- or Two-Dimensional Isotropic Heisenberg Models. *Phys. Rev. Lett.* **1966**, *17*, 1133–1136.
28. Bruno, P. Absence of Spontaneous Magnetic Order at Nonzero Temperature in One- and Two-Dimensional Heisenberg and XY Systems with Long-Range Interactions. *Phys. Rev. Lett.* **2001**, *87*, 137203.
29. Ferris, J. H.; Kushmerick, J. G.; Johnson, J. A.; Yoshikawa Youngquist, M. G.; Kessinger, R. B.; Kingsbury, H. F.; Weiss, P. S. Design, Operation, and Housing of an Ultrastable, Low Temperature, Ultrahigh Vacuum Scanning Tunneling Microscope. *Rev. Sci. Instrum.* **1998**, *69*, 2691–2695.
30. Ulman, A. Formation and Structure of Self-Assembled Monolayers. *Chem. Rev.* **1996**, *96*, 1533–1554.
31. Smith, R. K.; Lewis, P. A.; Weiss, P. S. Patterning Self-Assembled Monolayers. *Prog. Surf. Sci.* **2004**, *75*, 1–68.
32. Love, J. C.; Estroff, L. A.; Kriebel, J. K.; Nuzzo, R. G.; Whitesides, G. M. Self-Assembled Monolayers of Thiolates on Metals as a Form of Nanotechnology. *Chem. Rev.* **2005**, *105*, 1103–1169.
33. Weiss, P. S. Functional Molecules and Assemblies in Controlled Environments: Formation and Measurements. *Acc. Chem. Res.* **2008**, *41*, 1772–1781.
34. Saavedra, H. M.; Mullen, T. J.; Zhang, P. P.; Dewey, D. C.; Claridge, S. A.; Weiss, P. S. Hybrid Approaches in Nanolithography. *Rep. Prog. Phys.* **2010**, *73*, 036501.
35. Claridge, S. A.; Liao, W. S.; Thomas, J. C.; Zhao, Y.; Cao, H. H.; Cheunkar, S.; Serino, A. C.; Andrews, A. M.; Weiss, P. S. From the Bottom Up: Dimensional Control and Characterization in Molecular Monolayers. *Chem. Soc. Rev.* **2013**, *42*, 2725–2745.
36. Baše, T.; Bastl, Z.; Šlouf, M.; Klementová, M.; Šubrt, J.; Vetushka, A.; Ledinský, M.; Fejfar, A.; Macháček, J.; Carr, M. J.; et al. Gold Micrometer Crystals Modified with Carboranethiol Derivatives. *J. Phys. Chem. C* **2008**, *112*, 14446–14455.
37. Hohman, J. N.; Claridge, S. A.; Kim, M.; Weiss, P. S. Cage Molecules for Self-Assembly. *Mater. Sci. Eng., R* **2010**, *70*, 188–208.
38. Baše, T.; Bastl, Z.; Plzák, Z.; Grygar, T.; Plešek, J.; Carr, M. J.; Malina, V.; Šubrt, J.; Boháček, J.; Večerníková, E.; et al. Carboranethiol-Modified Gold Surfaces. A Study and Comparison of Modified Cluster and Flat Surfaces. *Langmuir* **2005**, *21*, 7776–7785.
39. Hohman, J. N.; Zhang, P.; Morin, E. I.; Han, P.; Kim, M.; Kurland, A. R.; McClanahan, P. D.; Balema, V. P.; Weiss, P. S. Self-Assembly of Carboranethiol Isomers on Au{111}: Intermolecular Interactions Determined by Molecular Dipole Orientations. *ACS Nano* **2009**, *3*, 527–536.
40. Dameron, A. A.; Charles, L. F.; Weiss, P. S. Structures and Displacement of 1-Adamantanethiol Self-Assembled Monolayers on Au{111}. *J. Am. Chem. Soc.* **2005**, *127*, 8697–8704.
41. Saavedra, H. M.; Barbu, C. M.; Dameron, A. A.; Mullen, T. J.; Crespi, V. H.; Weiss, P. S. 1-Adamantanethiolate Monolayer Displacement Kinetics Follow a Universal Form. *J. Am. Chem. Soc.* **2007**, *129*, 10741–10746.
42. von Wrochem, F.; Scholz, F.; Gao, D.; Nothofer, H.-G.; Yasuda, A.; Wessels, J. M.; Roy, S.; Chen, X.; Michl, J. High-Band-Gap Polycrystalline Monolayers of a 12-Vertex *p*-Carborane on Au(111). *J. Phys. Chem. Lett.* **2010**, *1*, 3471–3477.
43. Spokoyny, A. M.; Machan, C. W.; Clingerman, D. J.; Rosen, M. S.; Wiester, M. J.; Kennedy, R. D.; Stern, C. L.; Sarjeant, A. A.; Mirkin, C. A. A Coordination Chemistry Dichotomy for Icosahedral Carborane-Based Ligands. *Nat. Chem.* **2011**, *3*, 590–596.
44. Wiesendanger, R.; Eng, L.; Hidber, H. R.; Oelhafen, P.; Rosenthaler, L.; Staufer, U.; Güntherodt, H. J. Local Tunneling Barrier Height Images Obtained with the Scanning Tunneling Microscope. *Surf. Sci.* **1987**, *189−190*, 24–28.
45. Olesen, L.; Brandbyge, M.; Sørensen, M.; Jacobsen, K.; Lægsgaard, E.; Stensgaard, I.; Besenbacher, F. Apparent Barrier Height in Scanning Tunneling Microscopy Revisited. *Phys. Rev. Lett.* **1996**, *76*, 1485–1488.
46. Rusu, P.; Brocks, G. Work Functions of Self-Assembled Monolayers on Metal Surfaces by First-Principles Calculations. *Phys. Rev. B* **2006**, *74*, 073414.
47. Jain, J.; Jain, A. Displacement Measurement and Its Application in Interframe Image Coding. *IEEE Trans. Commun.* **1981**, *29*, 1799–1808.
48. Love, N. S.; Kamath, C. An Empirical Study of Block Matching Techniques for the Detection of Moving Objects. *Proc. SPIE* **2006**, 1–36.
49. Kristiansen, K.; Stock, P.; Baimpos, T.; Raman, S.; Harada, J. K.; Israelachvili, J. N.; Valtiner, M. Influence of Molecular Dipole Orientations on Long-Range Exponential Interaction Forces at Hydrophobic Contacts in Aqueous Solutions. *ACS Nano* **2014**, *8*, 10870–10877.
50. Metropolis, N.; Rosenbluth, A. W.; Rosenbluth, M. N.; Teller, A. H.; Teller, E. Equation of State Calculations by Fast Computing Machines. *J. Chem. Phys.* **1953**, *21*, 1087–1092.
51. Pascual, J.; Jackiw, J.; Kelly, K.; Conrad, H.; Rust, H. P.; Weiss, P. S. Local Electronic Structural Effects and Measurements on the Adsorption of Benzene on Ag(110). *Phys. Rev. B* **2000**, *62*, 12632–12635.
52. Claridge, S. A.; Thomas, J. C.; Silverman, M. A.; Schwartz, J. J.; Yang, Y.; Wang, C.; Weiss, P. S. Differentiating Amino Acid Residues and Side Chain Orientations in Peptides Using

Scanning Tunneling Microscopy. *J. Am. Chem. Soc.* **2013**, *135*, 18528–18535.
53. Kim, J.; Rim, Y. S.; Liu, Y.; Serino, A. C.; Thomas, J. C.; Chen, H.; Yang, Y.; Weiss, P. S. Interface Control in Organic Electronics Using Mixed Monolayers of Carboranethiol Isomers. *Nano Lett.* **2014**, *14*, 2946–2951.
54. Stranick, S. J.; Parakh, A. N.; Tao, Y.-T.; Allara, D. L.; Weiss, P. S. Phase Separation of Mixed-Composition Self-Assembled Monolayers into Nanometer Scale Molecular Domains. *J. Phys. Chem.* **1994**, *98*, 7636–7646.
55. Smith, R. K.; Reed, S. M.; Monnel, J. D.; Lewis, P. A.; Clegg, R. S.; Kelley, K. F.; Bumm, L. A.; Hutchison, J. E.; Weiss, P. S. Phase Separation within a Binary Self-Assembled Monolayer on Au{111} Driven by an Amide-Containing Alkanethiol. *J. Phys. Chem. B* **2001**, *15*, 1119–1122.
56. Hampton, J. R.; Dameron, A. A.; Weiss, P. S. Double-Ink Dip-Pen Nanolithography Studies Elucidate Molecular Transport. *J. Am. Chem. Soc.* **2006**, *128*, 1648–1653.
57. Nuzzo, R. G.; Dubois, L. H.; Allara, D. L. Fundamental Studies of Microscopic Wetting on Organic-Surfaces. 1. Formation and Structural Characterization of a Self-Consistent Series of Polyfunctional Organic Monolayers. *J. Am. Chem. Soc.* **1990**, *112*, 558–569.
58. Poirier, G. E. Characterization of Organosulfur Molecular Monolayers on Au(111) using Scanning Tunneling Microscopy. *Chem. Rev.* **1997**, *97*, 1117–1127.
59. Dameron, A. A.; Charles, L. F.; Weiss, P. S. Structures and the Displacement of 1-Adamantanethiol Self-Assembled Monolayers on Au{111}. *J. Am. Chem. Soc.* **2005**, *127*, 8697–9704.
60. Kim, M. H.; Hohman, J. N.; Morin, E. I.; Daniel, T. A.; Weiss, P. S. Self-Assembled Monolayers of 2-Adamantanethiol on Au{111}: Control of Structure and Displacement. *J. Phys. Chem. A* **2012**, *113*, 3895–3903.
61. Stipe, B. C.; Rezaei, M. A.; Ho, W. Single-Molecule Vibrational Spectroscopy and Microscopy. *Science* **1998**, *280*, 1732–1735.
62. Khuong, T. A. V.; Nunez, J. E.; Godinez, C. E.; Garcia-Garibay, M. A. Crystalline Molecular Machines: A Quest toward Solid-State Dynamics and Function. *Acc. Chem. Res.* **2006**, *39*, 413–422.
63. Michl, J.; Sykes, C. H. Molecular Rotors and Motors: Recent Advances and Future Challenges. *ACS Nano* **2009**, *3*, 1042–1048.
64. Lee, H. J.; Ho, W. Structural Determination by Single-Molecule Vibrational Spectroscopy and Microscopy: Contrast between Copper and Iron Carbonyls. *Phys. Rev. B* **2000**, *61*, 347–350.
65. Lewis, P. A.; Inman, C. E.; Maya, F.; Tour, J. M.; Hutchison, J. E.; Weiss, P. S. Molecular Engineering of the Polarity and Interactions of Molecular Electronics Switches. *J. Am. Chem. Soc.* **2005**, *127*, 17421–17426.
66. Baber, A. E.; Jensen, S. C.; Sykes, E. C. H. Dipole-Driven Ferroelectric Assembly of Styrene on Au{111}. *J. Am. Chem. Soc.* **2007**, *129*, 6368–6369.
67. Han, P.; Akagi, K.; Canova, F. F.; Mutoh, H.; Shiraki, S.; Iwaya, K.; Weiss, P. S.; Asao, N.; Hitosugi, T. Botton-Up Graphene-Nanoribbon Fabrication Reveals Chiral Edges and Enantioselectivity. *ACS Nano* **2014**, *8*, 9181–9187.
68. Ferris, J. H.; Kushmerick, J. G.; Johnson, J. A.; Yoshikawa Youngquist, M. G.; Kessinger, R. B.; Kingsbury, H. W.; Weiss, P. S. Design, Operation, and Housing of an Ultrastable, Low Temperature, Ultrahigh Vacuum Scanning Tunneling Microscope. *Rev. Sci. Instrum.* **1998**, *69*, 2691–2695.
69. Monnell, J. D.; Stapleton, J. J.; Dirk, S. M.; Reinerth, W. A.; Tour, J. M.; Allara, D. L.; Weiss, P. S. Relative Conductances of Alkaneselenolate and Alkanethiolate Monolayers on Au{111}. *J. Phys. Chem. B* **2005**, *109*, 20343–20349.
70. Chan, M. H.; Yu, Y. B.; Constantinides, A. G. Variable Size Block Matching Motion Compensation with Applications to Video Coding. *Proc. Inst. Elec. Eng.* **1990**, *137*, 205–212.
71. Nie, Y.; Ma, K. K. Adaptive Rood Pattern Search for Fast Block-Matching Motion Estimation. *IEEE Trans. Image Process.* **2002**, *11*, 1442–1449.